White Rose Research Online

eprints@whiterose.ac.uk
https://eprints.whiterose.ac.uk
Universities of Leeds, Sheffield and York

Deposited via The University of Leeds.

White Rose Research Online URL for this paper:
https://eprints.whiterose.ac.uk/id/eprint/85963/

Version: Accepted Version

Article:
Skelton, R and Walker, AM (2015) The effect of cation order on the elasticity of omphacite from atomistic calculations. Physics and Chemistry of Minerals, 42 (8). pp. 677-691. ISSN: 0342-1791

https://doi.org/10.1007/s00269-015-0754-9

Reuse
Items deposited in White Rose Research Online are protected by copyright, with all rights reserved unless indicated otherwise. They may be downloaded and/or printed for private study, or other acts as permitted by national copyright laws. The publisher or other rights holders may allow further reproduction and re-use of the full text version. This is indicated by the licence information on the White Rose Research Online record for the item.

Takedown
If you consider content in White Rose Research Online to be in breach of UK law, please notify us by emailing eprints@whiterose.ac.uk including the URL of the record and the reason for the withdrawal request.

UNIVERSITY OF LEEDS
University of Sheffield
UNIVERSITY of York

The effect of cation order on the elasticity of omphacite from atomistic calculations

Richard Skelton[a,*] and Andrew M. Walker[b,c]

[a] Research School of Earth Sciences, Australian National University, Canberra, ACT, 0200, Australia

[b] School of Earth Sciences, University of Bristol, Wills Memorial Building, Queens Road, Bristol, BS8 1RJ, UK

[c] now at School of Earth and Environment, University of Leeds, Leeds, LS2 9JT, UK

* Corresponding author: richard.skelton@anu.edu.au

Abstract

Omphacite, a clinopyroxene mineral with two distinct crystallographic sites, M1 and M2, and composition intermediate between diopside and jadeite, is abundant throughout the Earth's upper mantle, and is the dominant mineral in subducted oceanic crust. Unlike the end-members, omphacite exists in two distinct phases, a P2/n ordered phase at low temperature and a high-temperature C2/c disordered phase. The crystal structure and full elastic constants tensor of ordered P2/n omphacite have been calculated to 15 GPa using plane-wave density functional theory. Our results show that several of the elastic constants, notably C_{11}, C_{12}, and C_{13} deviate from linear-mixing between diopside and jadeite. The anisotropy of omphacite decreases with increasing pressure and, at 10 GPa, is lower than that of either diopside or jadeite. The effect of cation disorder is investigated through force-field calculations of the elastic constants of Special Quasirandom

Structures supercells with simulated disorder over the M2 sites only, and over both cation sites. These show that cation order influences the elasticity, with some components displaying particular sensitivity to order on a specific cation site. C_{11}, C_{12}, and C_{66} are sensitive to disorder on M1, while C_{22} is softened substantially by disorder on M2, but insensitive to disorder on M1. This shows that the elasticity of omphacite is sensitive to the degree of disorder, and hence the temperature. We expect these results to be relevant to other minerals with order-disorder phase transitions, implying that care must be taken when considering the effects of composition on seismic anisotropy.

Keywords

Elasticity; Omphacite; Cation Order; Special Quasirandom Structures; Density functional theory

1. Introduction

Diopside-rich clinopyroxenes are a major component of the Earth's upper mantle, comprising ~20% of the region's total volume (Herzberg 1995). The proportion of clinopyroxene in eclogite, the principal component of subducted oceanic crust, is even higher, reaching up to ~65% by volume, although this proportion drops rapidly above 10 GPa, where clinopyroxene dissolves into garnet, the other major component of eclogite (Irifune et al. 1986; Irifune and Ringwood 1987; Irifune and Ringwood 1993). In natural eclogites, such as those that occur in the mantle and subducted oceanic crust, garnet exhibits weak crystallographic preferred orientation (CPO) and is essentially elastically isotropic (Bascou et al. 2001; Mainprice et al. 2004). In contrast, omphacite has pronounced shear-induced CPO, with the [001] axis parallel to the direction of greatest elongation (Mauler et al. 2001; Bascou et al. 2002). Consequently, seismic anisotropy in eclogitic rocks is dominated by the behaviour of omphacite (Mauler et al. 2000; Bascou et al. 2001; Zhang and Green 2007). It has

been suggested that cation order affects the development of CPO in omphacite (Brenker et al. 2002), although this conclusion has been disputed (Ulrich and Mainprice 2005). It is possible that cation order influences the elastic properties of omphacite.

Like other clinopyroxenes, omphacite (shown in Fig. 1) is a monoclinic silicate mineral with four formula units per unit cell and the general composition $M1M2Si_2O_6$, where M1 and M2 are metallic cations occupying crystallographically distinct sites. The M2 site is occupied by either Ca^{2+} or Na^{+}, while the M1 site is occupied by Mg^{2+} or Al^{3+}, with the amount of each cation determined by charge balance considerations. The primary structural features of omphacite are chains of corner-linked SiO_4 tetrahedra and edge-sharing $M1O_6$ octahedra, both of which lie parallel to the *c*-axis. As in jadeite and diopside, the M2 cations occupy irregular eight-fold coordinated sites, which are more compressible than either the M1 or Si sites (Levien and Prewitt 1981). Naturally occurring omphacite has two distinct phases: a low temperature, ordered phase with space group P2/n and a high temperature, disordered phase with space group C2/c (Carpenter 1980).

In the P2/n structure, cation ordering causes the M1 and M2 sites to split into two sub-sites each, labelled M11 and M12, and M21 and M22, respectively. Mg^{2+} preferentially occupies the M11 sub-site, while Ca preferentially occupies the M22 sub-site. At all temperatures where the P2/n phase is stable, the M11 and M22 sub-sites are more ordered than the M21 and M22 sub-sites. It has been observed in both experimental (Boffa Ballaran et al. 1998) and computational (Vinograd et al. 2007) studies that, at moderate temperatures, the relationship between cation order on the two sites closely follows $Q_{M1} = 2\ Q_{M2}$, where Q_{M1} and Q_{M2} are the long range order parameters of the M1 and M2 sites, respectively.

While it has been suggested that this ordering scheme is required for local charge balance (Rossi et al. 1983), recent calculations predict that the stable structure at zero Kelvin should be completely ordered (Burton and Davidson 1988; Vinograd 2002a; Vinograd 2002b). However, the slow kinetics of cation diffusion in omphacite at low temperature inhibits the ordering process, and natural omphacite always possess some cation disorder (Carpenter 1978). Vinograd et al. (2007) compared order parameters calculated using Monte Carlo simulations with values obtained for a natural omphacite (Boffa Ballaran et al. 1998), and concluded that cation ordering is kinetically ineffective below 600 °C. The order parameters decrease systematically to ~850 °C, where both order parameters are effectively zero.

Despite their abundance, the elastic properties of the clinopyroxene minerals remain poorly understood, due primarily to the low symmetry of the clinopyroxenes, and their correspondingly large number of independent elastic constants, which makes experimental measurements difficult at mantle pressures (Mainprice 2007). Consequently, existing studies have primarily focused on the elastic properties of clinopyroxenes at ambient pressure. Brillouin scattering has been used to measure the elastic constants of jadeite at ambient temperature and pressure (Kandelin and Weidner 1988), and of diopside at room pressure and ambient (Levien et al. 1979) and high temperature (Isaak et al. 2006). Brillouin scattering has recently been used to measure the individual elastic constants of single-crystal diopside to 14 GPa (Sang and Bass 2014), and were found to be consistent with earlier measurements of polycrystal bulk and shear moduli (Li and Neuville 2010). Measurements of the elastic constants of omphacite are even more limited in number, essentially restricted to the Brillouin scattering study of Bhagat et al. (1992), who measured elastic constants of a single-crystal of disordered omphacite at ambient temperature and pressure. Comparing their results with data for jadeite and diopside, they concluded that the elastic constants were not

85 significantly different from those predicted by linear mixing (between diopside and jadeite), except
86 for C_{22}, which was softer by ~9 GPa. Linear mixing was also found for a diopside rich natural
87 clinopyroxene solid solution although, once again, the cation sites were completely disordered
88 (Collins and Brown 1998). While the effect of order on the elasticity of omphacite has not been
89 measured, resonant ultrasound spectroscopic measurements on spodumene ($LiAlSi_2O_6$) through an
90 ordering transition (from spacegroup C2/c to $P2_1/c$) demonstrate that its elastic constants are
91 discontinuous across the phase transition (Sondergeld et al. 2006). It was suggested by Sondergeld
92 et al. that similar discontinuities may be observed across order-disorder phase boundaries in mantle
93 clinopyroxenes.

94 Computational methods do not have the same limitations, and have been used to calculate the high-
95 pressure elastic constants of clinopyroxenes, particularly jadeite and diopside. The first such study
96 was due to Matsui and Busing (1984), who used a simple set of interatomic potentials to calculate
97 the elastic constants of diopside to 5 GPa. More recently, density functional theory (DFT;
98 Hohenberg and Kohn 1964; Kohn and Sham 1965) has been used to calculate the structure and
99 elastic constants of diopside ($CaMgSi_2O_6$) and jadeite ($NaAlSi_2O_6$) to 20 GPa (Walker 2012).
100 However, these studies have focused exclusively on clinopyroxenes with end-member
101 compositions, while mantle clinopyroxenes invariably occur as solid solutions.

102 Substitutional systems, including alloys and solid solutions, are typically disordered, and lack
103 translational symmetry, making them difficult to model using computational methods such as DFT,
104 which use periodic boundary conditions. Many techniques have been developed to calculate the
105 properties of substitutional systems but, due to the large number of possible configurations of an
106 alloy, these techniques invariably involve significant trade-off between accuracy and computational

cost. Some methods, including the virtual crystal approximation (Bellaiche and Vanderbilt 2000) and the coherent-potential approximation (Faulkner and Stocks 1980) treat the crystal as an average over all possible configurations. Consequently these methods can use small simulation cells, at the cost of neglecting the effects of local strain on the energy of a specific configuration, which may be significant for substitutional systems in which mixing is accommodated by local relaxation. A recently developed method, based on averages over symmetry-irreducible classes of atomic configurations (Mustapha et al. 2013; D'Arco et al. 2013; Lacivita et al. 2014), permits the inclusion of local relaxation, although at the cost of a greater number of calculations relative to the virtual crystal or coherent potential approximations. Cluster expansion calculations, in which the properties of a solid solution are expanded in terms of the properties of "clusters" of atomic sites, incorporate the effects of local relaxation (Laks et al. 1992). Although originally developed to model scalar properties, the cluster expansion formalism can be extended to tensor-valued quantities, including the elasticity tensor (van de Walle 2008), although at significant computational cost. Another approach to modelling alloys and solid solutions is the Special Quasirandom Structures method (SQS; Zunger et al. 1990), in which the atoms in a supercell are arranged such that the correlations between the occupancies of different sites in a cluster are as close as possible to those of a truly random alloy. In practice, only a finite number of clusters are used, as the properties of the alloy are assumed to be controlled by short-ranged few-body correlations. By looking for the cell that most closely approximates the statistical properties of a disordered material, the properties of the random alloy can be computed by considering only a single simulation cell of finite size, with periodic boundary conditions. This permits calculations to be carried out at relatively low computational cost without neglecting the contribution of local relaxation to the structure and energetics of the configuration.

In this study, the effect of cation disorder on the elastic constants of omphacite at mantle pressure is investigated using *ab initio* density functional theory calculations and parameterized interatomic potentials. The effect of pressure on the elastic constants of the ordered phase of omphacite is established using plane-wave DFT calculations at a range of upper mantle pressures. To investigate the effect of cation disorder on the elastic constants, disordered supercells are prepared using the SQS method. As these supercells are necessarily much larger than the unit cell, the computational cost of DFT is prohibitive. We thus turn to a parameterised interatomic potential model, developed by Vinograd et al. (2007) to study the energetics and thermodynamics of cation ordering in omphacite, to calculate the elastic constants of the SQS supercells. Two disordering scenarios are considered: disorder on M2 but not M1, corresponding to the intermediate temperature case, and a fully disordered structure, corresponding to the high-temperature C2/c phase. As both experiments (eg. Rossi et al. 1983; Boffa Ballaran et al. 1998) and simulations (Vinograd et al. 2007) have shown that the M2 site is always more disordered than the M1 site, we do not here consider the effect of disorder on M1 in the absence of disorder on M2. As we are concerned specifically with the effect of cation disorder on the elasticity of omphacite, we neglect all thermo-elastic effects when calculating elastic constants.

2. Methodology

Ab initio Calculations

The elastic constants of the P2/n structure were calculated using plane-wave DFT with the pseudopotential approximation, as implemented in the Quantum Espresso software package (Giannozzi et al. 2009). The PW91 GGA exchange-correlation (xc) functional (Perdew 1991;

149 Perdew et al. 1992) was used in all calculations. For all calculations, we used a 2 x 2 x 4
150 Monkhorst-Pack grid (Monkhorst and Pack 1976) and a cutoff for the plane wave basis of 60 Ry
151 (~815 eV), giving well-converged values for the total energy and structure of the unit cell, as well
152 as the forces on individual atoms. Core electrons were treated using Vanderbilt ultrasoft
153 pseudopotentials (Vanderbilt 1990), with the *3s3p4s*, *2s2p*, *3s3p*, *2p3s*, *3s3p*, and *2s2p3s* electrons
154 treated as valence for Ca, O, Si, Mg, Al and Na, respectively. Cell parameters and atomic
155 coordinates were relaxed in variable-cell calculations using the damped Wentzcovitch algorithm
156 (Wentzcovitch et al. 1993; Wentzcovitch et al. 1995).

157 The full elastic constants matrix was calculated by applying a strain to the unit cell and calculating
158 the resulting stress, from which the elastic constants could be found using the Hooke's Law linear
159 stress-strain relationship (eg. Wentzcovitch et al. 1995; Karki et al. 1999; Stackhouse et al. 2005;
160 Perger et al. 2009). For monoclinic crystals, symmetry constraints reduce the number of
161 independent elastic constants to just 13, rather than the full set of 21 for a triclinic crystal. These can
162 be calculated using just four distinct strain patterns (Walker 2012). As Hooke's Law breaks down at
163 large strain amplitudes, the magnitude δ of the applied strain must be relatively small so that stress
164 and strain are linearly related. Conversely, if δ is too small, the errors introduced by the finite
165 convergence criteria used in the DFT calculation will be of the same order of magnitude as the
166 induced stress, leading to poorly constrained values of the elastic constants. In this study, strains
167 were applied at the six magnitudes +-0.03333 a.u., +-0.06666 a.u and +-0.1 a.u.

Special Quasirandom Structures

168 In this study, the SQS method was used to simulate the effects of disordering of the M1 and M2

cation sites on the elasticity of omphacite. For calculations performed with periodic boundary conditions, the finite size of the simulation cell introduces artificial intersite correlations. The SQS method arranges atoms in a supercell such that intersite occupation correlations are as close as possible to those of a random alloy. For small supercell size, SQS supercells can be generated through exhaustive enumeration of all possible supercell configurations, but this scales factorially with the number of interchangeable sites, and is computationally prohibitively expensive for large supercell sizes. SQS supercells of various sizes were generated using `mcsqs` program (van de Walle et al. 2013), part of the Alloy Theoretic Automated Toolkit (van de Walle et al. 2002; van de Walle 2009). The `mcsqs` algorithm finds the supercell of the specified size which is most similar to a random alloy, in the sense that a specified set of intersite correlation functions are close to those of a random alloy. This minimises the error associated with correlated occupancies caused by the use of periodic boundary conditions, and allows us to find the properties of a random alloy by performing calculations on a single structure of finite size. For fitting of the SQS structure, we used all two-body clusters with diameter less than 9.0 Å, along with all three-body clusters with diameter less than 5.0 Å. These are precisely the diameters at which the effective cluster interactions calculated by Vinograd et al. (2007) for the diopside-omphacite-jadeite system are effectively zero, suggesting no coupling between sites.

Having generated an SQS supercell, its elastic constants can be calculated using any of the standard methods used in computational materials science. In this study, due to the large size of the SQS supercell required to converge the elastic constants and the poor (N^3) scaling of DFT with system size, calculations were performed using molecular mechanics force-fields, as implemented in GULP (Gale 1997; Gale and Rohl 2003), with the interatomic potentials of Vinograd et al. (2007), which has previously been used to study order-disorder phenomena in the diopside-jadeite system. This

192 model uses the shell model to simulate oxygen polarizability (Dick and Overhauser 1958),
193 Buckingham potentials for the interactions between oxygen shells and cations, and three body
194 potentials to constrain bond angles in the SiO_4 tetrahedra and the AlO_6 and MgO_6 octahedra. Ionic
195 charges are set equal to 0.85 times the formal charge, which has been shown to improve the
196 transferability of these potentials for oxides and silicates (Vinograd et al. 2004; Vinograd et al.
197 2006).

198 Due to the finite size of the simulation cells used, generated SQS supercells typically belong to a
199 lower symmetry class than would an ideal disordered crystal of the same composition (Tasnádi et
200 al. 2012), with a corresponding increase in the number of non-zero elastic constants. To obtain
201 approximate values for the elastic constants in the true symmetry class of the disordered crystal, the
202 calculated elasticity tensor must be projected into a tensor with the desired symmetry properties
203 (Moakher and Norris 2006). This may be done by mapping the elastic constants matrix into the 21
204 dimensional vector

$$\boldsymbol{C} = (C_{11}, C_{22}, C_{33}, \sqrt{2}C_{23}, \sqrt{2}C_{13}, \sqrt{2}C_{12}, 2C_{44}, 2C_{55}, 2C_{66}, 2C_{14}, 2C_{25}, 2C_{36}, 2C_{34}, 2C_{15}, 2C_{26}, 2C_{24}, 2C_{35}, 2C_{16}, 2\sqrt{2}C_{56}, 2\sqrt{2}C_{46}, 2\sqrt{2}C_{45}) \quad (1)$$

205

206 Where the constant factors are there to ensure invariance of the Euclidean norm. The closest elastic
207 tensor with a high point group symmetry, in the sense that $\|\boldsymbol{C} - \boldsymbol{C}^{sym}\|$ is minimized, is found by
208 applying a 21 x 21 projection matrix $\mathbf{P}^{sym}$ to the elastic constants vector $\boldsymbol{C}$, giving

$$\boldsymbol{C}^{sym} = \boldsymbol{P}^{sym} \cdot \boldsymbol{C} \quad (2)$$

209

210 For crystals with monoclinic symmetry, $\mathbf{P}^{sym}$ is quite simple, with all off-diagonal terms equal to
211 zero, $\boldsymbol{P}_{ii}^{sym} = 0$ if i=10, 11, 13, 14, 16, 17, 19 or 20, and all other diagonal entries equal to 1
212 (Browaeys and Chevrot 2004). This method has previously been used to model the elastic constants
213 of several random alloys, including $Cr_{1-x}Al_xN$ (Zhou et al. 2013), $In_xAl_{1-x}N$ (Xie et al. 2012), and
214 $(Al_x,Mg_{1-x})Sc$ (Saha and Zwanziger 2014).

3. Results and Discussion

High pressure elasticity

215 Before considering the effects of cation disorder on the elastic properties of omphacite, we calculate
216 the elastic of the fully ordered structure using DFT. The elastic constants of P2/n omphacite at zero
217 applied pressure calculated in this study are listed in Table 1, together with the zero-pressure elastic
218 constants of diopside and jadeite calculated by Walker (2012), also using plane-wave DFT. All
219 reported uncertainties are fitting errors, and larger, systematic errors are likely to be present, in
220 particular those due to the underbinding of the GGA xc-functional. The underbinding of GGA can
221 be corrected through the application of an Empirical Energy Correction (eg. Otero-de-la-Roza and
222 Luaña 2011a; Otero-de-la-Roza and Luaña 2011b; Luo et al. 2013). The simplest such correction is
223 the PSHIFT EEC, in which an additional term $E_{correction} = P_{shift}V$ is added to the energy of the cell
224 (Otero-de-la-Roza et al. 2011). In the case of GGA functionals, $P_{shift} > 0$, reducing the unit cell

225 volume at constant pressure. This correction works because the energy derivatives as a function of
226 volume are reproduced more accurately than the cell volume as function of pressure (Vanderbilt
227 1998), and has seen wide application in the computational mineral physics (eg. Oganov et al. 2001;
228 Walker et al. 2008; Li et al. 2014). In the absence of low-temperature cell-volume data for P2/n
229 omphacite, we have calculated the empirical pressure correction by comparing the calculated cell
230 volumes with those obtained using X-ray powder diffraction for a natural ordered omphacite at
231 room temperature (Pavese et al. 2001), corrected to 0 K using the volumetric thermal expansion
232 coefficient of $\alpha_V = 2.58 \times 10^{-5}\ K^{-1}$ found for P2/n omphacite in a recent study (Pandolfo et al. 2014).
233 Note that since the volumetric thermal expansion vanishes as the temperature approaches 0 K, the
234 cell volumes used here are slightly too small, resulting in marginal overestimation of the pressure
235 correction. Comparing the calculated and experimental cell volumes (Fig. 2), the necessary pressure
236 correction is found to be 4.47 GPa, very close to the average of the pressure corrections of 4.30 GPa
237 for jadeite and 4.66 GPa for diopside found by Walker (2012) using the PBE exchange correlation
238 functional (Perdew et al. 1996), consistent with previous findings that the PSHIFT EEC for a
239 material of intermediate composition can be obtained as a composition weighted average of EECs
240 for end-member compositions (van de Walle and Ceder 1999). The applied pressure minus the
241 calculated pressure correction will be referred to throughout the rest of this paper as the 'nominal
242 pressure,' and it is this value that is most relevant for comparisons with experimental data.

243 As can be seen from the final column of Table 2, the isotropic bulk and shear moduli of P2/n
244 omphacite are broadly consistent with linear mixing between diopside and jadeite, as are many of
245 the individual elastic constants. However, several of the elastic constants deviate measurably from
246 linear mixing, in particular C_{23} which is softer than predicted from linear mixing by 5.0 GPa, and
247 C_{11}, C_{12}, and C_{13}, which are 7.6, 7.7, and 10.6 GPa stiffer than predicted, respectively. In fact, not

248 only do the calculated values for C_{12} and C_{13} exceed the linear mixing predictions, they are greater
249 than the corresponding values calculated for either diopside or jadeite.

250 The pressure evolution of the calculated elastic constants of P2/n omphacite is presented in Fig. 3.
251 At all nominal pressures greater than 0 GPa, C_{11} is the stiffest of the longitudinal constants, while
252 C_{22} is the softest. While the majority of the elastic constants stiffen as the pressure increases, the
253 pressure derivatives of C_{15}, C_{25}, C_{35}, and C_{46} are negative, with the values of C_{15} and C_{46}
254 converging on zero at high pressure. This is broadly similar to the reported high pressure behaviour
255 of diopside (Walker 2012; Sang and Bass 2014) although, in the case of P2/n omphacite, the value
256 of C_{25} remains positive even at high pressure.

257 Clinopyroxenes are of particular interest in seismological studies because of their high degree of
258 anisotropy. There are a number of ways to measure the elastic anisotropy of a low-symmetry
259 crystal, including the Universal Anisotropy Index (Ranganathan and Ostoja-Starzewski 2008),
260 defined as

$$A^U = 5\frac{G^R}{G^V} + \frac{K^R}{K^V} - 6 \quad (3)$$

261

262 where G is the shear modulus, K is the bulk modulus and the superscripts R and V refer to the
263 Reuss (homogeneous stress) and Voigt (homogeneous strain) bounds, respectively. Using the elastic
264 constants calculated in this study (Fig. 3), we find that the anisotropy of P2/n omphacite, as

measured by A^U, decreases monotonically with increasing pressure, from 0.421 at 0.526 GPa nominal pressure to 0.297 at 10.526 GPa. By way of comparison, a previous DFT study found that A^U equals 0.495 and 0.334 at 0 GPa nominal pressure for diopside and jadeite, respectively, decreasing to 0.383 and 0.382 at 10 GPa (Walker 2012), while the elastic constants of diopside found in a Brillouin scattering study using a single crystal of diopside (Sang and Bass 2014) give A^U = 0.343 at 0 GPa, decreasing to 0.21 at 10.5 GPa. The significant differences between the elastic constants of diopside found using DFT (Walker 2012) and Brillouin scattering (Sang and Bass 2014), seemingly due to disagreement between the values of the off-diagonal components of the elastic constants matrix, make determining the relative anisotropy of P2/n omphacite and the two end-member clinopyroxenes difficult, and lead to different conclusions about their relative anisotropy at high pressure. However, given that this study has used plane-wave DFT to calculate the elastic constants, we suggest that the most appropriate comparison is with the calculations of Walker (2012), indicating that, at low pressure, P2/n omphacite is more anisotropic than jadeite but less anisotropic than diopside, but is less anisotropic than either end-member at high pressure. This conclusion is supported by the maximum *S*-wave anisotropy $aV_S = (V_{S1} - V_{S2})/\frac{1}{2}(V_{S1} + V_{S2})$, where V_{S1} and V_{S2} are the fast and slow S-wave velocities, which, at high pressure, is lower for P2/n omphacite than for either end-member, although the *P*-wave anisotropy differs little among the three clinopyroxenes.

Effect of cation disorder

Omphacite has two distinct cation sites over which cation mixing can occur (M1 and M2). Since the two sites have measurably different properties, with the M1 octahedra being more rigid and incompressible than the M2 polyhedra, disordering over each site might be expected to impact the

287 elastic constants differently. To determine the relative influence of ordering of the M1 site versus
288 the M2 site on the elasticity, we calculated the elastic constants for supercells with simulated
289 disorder over the M2 site only, and compared these with the elastic constants for a supercell with
290 both sites fully disordered. This is also a physically relevant comparison, as the M2 site disorders at
291 lower temperatures than the M1 site, and so there is a wide range of temperatures at which the
292 cation distribution over M2 sub-sites is substantially disordered, while M1 remains largely ordered.
293 Consequently, the first model can be thought of as approximating the situation at moderate
294 temperatures, where the M2 site is disordered, but the M1 site is still largely ordered, while the
295 second simulates full disorder over both cation sites, as would be expected at temperatures above
296 the P2/n → C2/c phase transition. As M1 is always more ordered than M2, we do not calculate the
297 elastic constants of an SQS supercell with full order on M2 and disorder on M1.

298 While Vinograd et al. (2007) showed that the cell parameters and atomic coordinates of
299 clinopyroxenes were well reproduced by their interatomic potentials, a more rigorous test of the
300 potentials is to compare calculated elastic constants with those obtained from the *ab initio*
301 calculations described in the previous section. As expected, since the elastic constants depend on
302 the second derivative of the internal energy and are consequently more sensitive to model
303 deficiencies, some of the elastic constants calculated in GULP (Table 2) deviate significantly from
304 the DFT calculations presented in Table 1. One of the most obvious differences is the anomalously
305 high values of C_{13} and C_{33} found for all three minerals, Given that the stiffness of the c-axis is
306 controlled by chains of SiO_4 tetrahedra (Pavese et al. 2000), this suggests that the charge of the Si
307 atoms (+3.4) may be somewhat too large. Conversely, the diagonal shear constants C_{44}, C_{55}, and C_{66}
308 are all somewhat underestimated, particularly for jadeite and P2/n omphacite. C_{11} and C_{22} are
309 overestimated by ~5% for diopside, but are well reproduced for both jadeite and P2/n omphacite.

310 The isotropic bulk modulus of P2/n omphacite calculated using GULP is 7% greater than the DFT
311 value. However, if the bulk modulus is recalculated using the values of C_{13} and C_{33} from the DFT
312 calculations (Table 1) and values for all other constants from Table 2, we obtain a value of K^{vrh} =
313 116.3 GPa, comparable to the value for DFT reported in Table 1. In Table 2, we also report the
314 calculated difference between the elastic constants of P2/n omphacite and those obtained from
315 linear mixing between diopside and jadeite. There are a number of differences between these values
316 and those obtained using DFT, with the most notable being that GULP predicts C_{11} to follow linear
317 mixing, and C_{15} to deviate substantially from it. However, aside from these discrepancies, the two
318 methods generally agree on the qualitative difference between the elasticity of P2/n omphacite and a
319 linear mixture of diopside and jadeite.

320 A comparison between the pressure evolution of the elastic constants calculated using interatomic
321 potentials (Fig. 4) and the pressure evolution calculated using plane-wave DFT (Fig. 3) shows that
322 the pressure derivatives of the elastic constants of omphacite are reasonably well reproduced by the
323 interatomic potentials. Computing the average values of the pressure derivatives for each elastic
324 constant over the pressure range 0-5 GPa using GULP and DFT. We find that both methods give the
325 same sign for each of the dC_{ij}/dP over this range, with the difference between average pressure
326 derivatives calculated using DFT and GULP being -0.7 for C_{11}, 1.2 for C_{12}, and 0.7 for C_{23}. The
327 magnitudes of all other differences are < 0.5. Additionally, GULP was able to correctly reproduce
328 the relative ordering of dC_{ij}/dP found with DFT for 74 of the 78 possible unique pairs of elastic
329 constants, with the only exceptions being C_{33} and C_{12}, C_{44} and C_{55}, C_{15} and C_{25}, and C_{15} and C_{46}.
330 Consequently, given the degree of approximation inherent to molecular mechanics, and the fact that
331 construction of SQS supercells involves changes in the distributions of cations relative to the
332 ordered structure, but not the number of each species present (or their coordination environment), it

was judged that the interatomic potentials of Vinograd et al. (2007) should be sufficiently accurate to provide a useful guide to the qualitative effect of cation order on the elastic constants of omphacite.

Since the SQS method was not originally developed to calculate tensor-valued properties, it is necessary to test the convergence of the elastic constants with increasing SQS supercell size, as insufficiently large supercells can be artificially anisotropic (Tasnádi et al. 2012). This is done for the two different disordering cases by calculating the normalized Euclidean distance

$$\|\boldsymbol{C} - \boldsymbol{C}^{4\times4\times4}\| / \|\boldsymbol{C}^{4\times4\times4}\| \quad (4)$$

between the calculated elastic constants of each generated SQS supercell and a 4x4x4 SQS supercell. Examining these distances as function of supercell size (Fig. 5), it can be seen that, in both cases (disorder on M2 and full disorder), the distance decreases markedly with increasing supercell size. The elasticity tensor of the supercell with disorder over M2 only converges more rapidly than that with disorder over both sites, with the absolute difference falling below 1 % when a 2x2x2 supercell is used, while the difference remains above 1% for supercells smaller than 3x3x3 in the case of full disorder over both sites. The convergence of individual elastic constants is more mixed, with some constants (eg. C_{11} and C_{55}) converging much faster than the full elasticity tensor while others, such as C_{66}, converging quite slowly. Nevertheless, the majority of the elastic constants were converged to within 1% by the 3x3x3 supercell. As such, all further calculations were performed using a 3x3x3 supercell containing 1080 atoms, including 108 M1 and M2 sites.

352 In Table 2, the calculated 0 GPa elastic constants are tabulated for the two different SQS supercells.
353 For comparison, we have also calculated the elastic constants for each disordering scenario using a
354 mean-field approach, in which mixing sites are treated as having multiples atoms with fractional
355 occupation present simultaneously, and the interatomic potentials are scaled according to

$$U_{ij\cdots m}^{m-f} = o_i o_j \cdots o_m U_{ij\cdots m} \quad (5)$$

356

357 where $o_i \in [0,1]$is the average occupancy factor of species i and $U_{ij...m}$ is an n-body interatomic
358 potential (Gale and Rohl 2003). These are listed in Table 2, alongside the corresponding SQS
359 results. For both disordering scenarios, the mean-field bulk and shear moduli are greater than the
360 values obtained using SQS, as are the majority of the individual elastic constants. Looking now at
361 the SQS results, it is seen the bulk modulus is relatively unchanged by disorder, while the shear
362 modulus softens moderately, particularly for the fully disordered supercell.

363 While the isotropic bulk and shear moduli are, at most, moderately sensitive to cation order, the
364 individual elastic constants of omphacite can be highly sensitive to cation order. Comparing the
365 elastic constants for P2/n omphacite calculated using GULP with the SQS results for the two
366 disordering scenarios (Table 2), it is clear that, while the elastic constants are generally softened
367 slightly as overall cation disorder increases, individual constants change significantly more than
368 others, often with a marked dependence on the order parameter of a specific cation site. To cite
369 specific examples, C_{11}, C_{12}, and C_{66} are essentially unchanged by disorder on M2 only, but soften

370 significantly when the M1 site is allowed to disorder as well. Other elastic constants soften upon
371 disorder of M2, but are unaffected by any further disorder on M1. This is true particularly of C_{22},
372 whose value at 0 GPa declines from 198.3 to 189.5 GPa going from complete order to disorder on
373 M2 only, but is only an additional 1.3 GPa softer (ie. effectively unchanged) when both cation sites
374 are fully disordered. Several of the elastic constants, such as C_{33} and C_{13}, do not seem to have any
375 particular dependence on the degree of disorder at either site.

376 To demonstrate that these results hold at mantle pressures, we extend these calculations to 10 GPa
377 and calculate the difference between the elastic constants of the P2/n phase displayed in Fig. 4 and
378 the elastic constants to the SQS supercells for the two disordering cases. Examining these values
379 (displayed in Fig. 6), it is immediately apparent that the differences at ambient pressure persist
380 across the entire pressure stability field for omphacite in the mantle. Moreover, the differences
381 between the elastic constants for the ordered and disordered structures change by less than ~1 GPa
382 over the pressure range studied, with few exceptions. The most obvious of these is C_{11} (the filled
383 squares in Fig. 6ac), whose sensitivity to cation order increases substantially over this range, with
384 the magnitude of its deviation from the value calculated for the P2/n structure tripling between 0
385 and 10 GPa when disorder occurs on M2 only, and increasing by a factor of ~2 for mixing over both
386 sites. C_{22} (filled diamonds) also exhibits anomalously high pressure sensitivity although, in its case,
387 the effect of increasing pressure is to reduce the difference between the ordered and disordered
388 values of this elastic constant.

389 Although relating changes in individual elastic constants to structural features is often difficult,
390 some of the differences noted above are due to the particular structural motifs of the clinopyroxene
391 structure. In particular, the fact that C_{11}, C_{12}, and C_{66} depend on the order parameter of the M1 site,

but not that of the M2 site is likely due to the moderate sensitivity of the *a* cell parameter to the occupancy of the M1 sites (Pavese et al. 2000). Conversely, since the stiffness of the c axis is controlled by the chains of SiO_4 tetrahedra (Pavese et al. 2000), C_{33} should have little direct dependence on the occupancies of either the M1 or M2 cation sites. This is in accord with the results presented in Table 2 and Fig. 6, where it can be seen that C_{33} is softened equally by disorder on each cation site, with the observed softening due exclusively to the dilation of the unit cell that accompanies cation disorder.

To demonstrate the effect that changing cation order can have on seismic wave-speeds and anisotropy, we calculate phase velocities for the quasi-*P,* and fast (V_{S1}) and slow (V_{S2}) quasi-*S* waves as a function of propagation direction for ordered, partially disordered, and fully disordered omphacite. The elastic constants for P2/n omphacite calculated using plane-wave DFT from Table 1 and, for each disordering case, add the difference between the elastic constants of the associated SQS supercell and P2/n omphacite calculated using interatomic potentials (Table 2). Pole figures of the quasi-P wave velocities, S-wave anisotropy aV_S, and fast quasi-S wave polarisation, calculated using the Matlab Seismic Anisotropy Toolkit (MSAT; Walker and Wookey, 2012), are plotted in Fig. 7. The effect of increasing cation disorder on the isotropic wave-speeds is negligible, with both *P*- and *S*-wave velocities varying by <2% between the P2/n and C2/c structures. In contrast, the magnitude and pattern of anisotropy appears to vary significantly with changing cation order. In particular, the *P*-wave anisotropy decreases by ~15 % going from the P2/n structure to full disorder over both cation sites. There is also a general reduction in aV_S, particularly in the equatorial plane containing the *b* and *c* lattice vectors.

These results are of direct relevance to the elasticity of mantle omphacites as the P2/n → C2/c

414 order-disorder phase transition has been found to occur at ~850 °C (Carpenter 1980), a conclusion
415 that is supported by Monte Carlo simulations using a cluster-expansion approach (Vinograd et al.
416 2007). At pressures sufficiently great for eclogite to form, temperatures in the interiors of old
417 subducted slabs, such as those beneath the Izu-Bonin or Tonga-Kermadec subduction zones, can be
418 as low as 400 °C (Peacock and Wang 1999; Abers et al. 2006; Syracuse et al. 2010). Indeed,
419 thermal modeling of the Nicaragua-Costa Rica subduction zone shows that, even at pressures in
420 excess of 6 GPa, temperatures at the center of a subducting slab may be <600 °C (Peacock et al.
421 2005). These temperatures lie well below the P2/n → C2/c order-disorder phase transition, and
422 suggest that omphacite is subducted slabs may be partially ordered to great depths, enhancing the
423 sensitivity of the pattern of anisotropy to the temperature of the slab interior.

424 Cation order has previously been found to affect the bulk and shear moduli of several major
425 minerals, including ringwoodite (Panero 2008) and $MgAl_2O_4$ spinel (eg. Cynn et al. 1993; Hazen
426 and Yang 1999; Li et al. 2007a). Sensitivity of the elastic constants to cation order has also been
427 documented for several garnets, including majorite (Li et al. 2007b) and grossular-andradite solid
428 solutions (eg. Babuška et al. 1978; O'Neill et al. 1989; Erba et al. 2014). In this last case, however,
429 a recent ab initio investigation has used averages over symmetry-independent classes of nuclear
430 configurations to determine the elastic behavior of solid solutions along the grossular-andradite
431 join, finding that the isotropic bulk and shear moduli follow a linear-mixing trend between the two
432 end-members (Lacivita et al. 2014).

433 In many of these studies, both the isotropic and anisotropic elastic moduli were sensitive to the
434 degree of cation order. For example, GGA-DFT calculations found that, for ringwoodite, a disorder
435 fraction of 0.125 is sufficient to reduce C_{11} from 323.4 GPa (ordered) to 301.5 GPa (disordered),

and to reduce the bulk modulus from 180 GPa to 166.8 GPa (Panero 2008). In some cases, however, the responses of the isotropic and anisotropic elastic moduli may diverge. Li et al. (2007b) found that many of the elastic constants of majorite, especially C_{66}, were sensitive to disordering of the Mg and Si cations, while the isotropic bulk and shear moduli were effectively independent of cation order. Similarly, the results presented here for omphacite show a limited dependence of the isotropic bulk and shear moduli on cation order (beyond the softening due to unit-cell dilation), but several of the individual elastic constants harden substantially as cation order increases. This illustrates a general point that, even in cases when the effect of cation order on the isotropic bulk and shear moduli is negligible, the individual elastic constants may be occupation-dependent, causing the anisotropy (and related phenomena such as S-wave splitting) to vary with changing cation order.

4. Conclusions

In this study, we have calculated the elastic constants of fully ordered omphacite using plane-wave DFT. It was found that many of the elastic constants are broadly consistent with linear mixing between diopside and jadeite, with several notable exceptions, including C_{11}, C_{12}, and C_{13}. While the anisotropy of omphacite was intermediate between that of diopside and jadeite at 0 GPa, it decreased rapidly with increasing temperature and, at 10 GPa, P2/n omphacite may be less anisotropic than either diopside or jadeite.

Using the SQS method, we demonstrated that the elastic constants of omphacite depend on the degree of cation disorder present at both the M1 and M2 sites. However, the relationship between the elasticity tensor and the total cation order was found to be non-trivial, with some elastic

constants (eg. C_{11}, C_{12}, and C_{66}) displaying particular sensitivity to the order parameter of the M1 site, while others (eg. C_{22}) are affected primarily by order on M2. Numerical simulations have suggested that temperatures in subducted oceanic crust at depths > 100 km can be as low as 400-600 °C (eg. Peacock and Wang 1999; Peacock et al. 2005), well below the temperature at which the P2/n → C2/c phase transition occurs. Indeed, an earlier computational study indicated that at these temperatures, although the M2 site is significantly disordered ($Q_{M2} < 0.6$), the M1 site should still be essentially fully ordered ($Q_{M1} > 0.9$) (Vinograd et al. 2007). Consequently, we expect that cation order in omphacite should affect the pattern and magnitude of seismic anisotropy in subducting slabs. Moreover, given that increasing cation disorder softens the elastic constants omphacite (with C_{23} the lone exception), we suggest that the seismic anisotropy of omphacite should more strongly temperature-dependent than a simple mechanical mixture of diopside and jadeite.

Acknowledgements

AMW is supported by a fellowship from the Natural Environment Research Council (Grant Number NE/K008803/1). Calculations were performed on the Terrawulf cluster, a computational facility supported through the AuScope initiative. AuScope Ltd is funded under the National Collaborative Research Infrastructure Strategy (NCRIS), an Australian Commonwealth Government Programme. Ian Jackson and two anonymous reviewers are thanked for their helpful comments.

Figure captions

Fig. 1 (a) Unit cell of omphacite, with the M11, M12, M21, and M22 cation sub-sites labeled. In

476 fully ordered P2/n omphacite, M11 is fully occupied by Mg^{2+}, M12 by Al^{3+}, M21 by Na^{+}, and M22
477 by Ca^{2+}. (b) The crystal structure viewed down the b-axis, which clearly shows the corner-linked
478 chains of SiO4 tetrahedra parallel to the c-axis. The crystal structure has been visualized using the
479 program Vesta 3 (Momma and Izumi 2011)

480 **Fig. 2** Uncorrected (triangles) and pressure-corrected (inverted triangles) cell volumes of P2/n
481 omphacite calculated using DFT, compared with experimental cell volume data (circles) taken from
482 (Pavese et al. 2001), corrected to 0 K using the volumetric thermal expansion coefficient from
483 (Pandolfo et al. 2014)

484 **Fig. 3** The elastic constants of P2/n omphacite as a function of pressure, calculated using plane-
485 wave DFT. (a) Longitudinal (Symbols: C_{11}, filled squares; C_{22}, filled diamonds; C_{33}, filled
486 triangles) and diagonal shear components of the elastic constants matrix C_{ij} (C_{44}, empty diamonds;
487 C_{55}, empty squares; C_{66}, empty inverted triangles). (b) Off-diagonal components of C_{ij} (Symbols:
488 C_{12}, filled squares; C_{13}, filled diamonds; C_{23}, filled triangles; C_{15}, empty diamonds; C_{25}, empty
489 squares; C_{35}, empty inverted triangles; C_{46}, filled inverted triangles). Calculated uncertainties are
490 smaller than the symbol size. Lines are a guide for the eye

491 **Fig. 4** (a) Bulk and diagonal shear components, and (b) off-diagonal shear components of the
492 elastic constants matrix of P2/n omphacite as a function of pressure, calculated in GULP using the
493 force-field model of Vinograd et al. (2007). The symbols are the same as those in Fig. 3. Lines are a
494 guide for the eye

495 **Fig. 5** Euclidean distance deviations between a 4x4x4 SQS supercell and smaller SQS supercells,

496 calculated using equation (4) for disorder over M2 only (hollow) and disorder over both sites
497 (filled)

498 **Fig. 6** Calculated difference between the elastic constants of the 3x3x3 SQS supercells with those of
499 the ordered P2/n phase. (a) and (c) show results for the diagonal components of the elastic constants
500 matrices in the case of disorder on M2 only and disorder on both sites, respectively. (b) and (d)
501 show the off-diagonal components, for disorder on M2 only and disorder on both sites. The symbols
502 are the same as those in Fig. 3. Lines are a guide for the eye

503 **Fig. 7** Wave velocities and anisotropy pole figures for (a) fully ordered omphacite (space group
504 P2/n) (b) omphacite with disorder on M2 only, and (c) fully disordered omphacite (space group
505 C2/c). Pole figures were calculated in MSAT (Walker and Wookey 2012) using the *ab initio* elastic
506 constants for P2/n omphacite presented in Table 1, with the effect of cation disorder simulated by
507 taking the difference between the elastic constants of ordered and disordered omphacite calculated
508 with SQS (Table 2). Cartesian coordinate system is shown in the inset, with *b* and *c* parallel to *X2*
509 and *X3,* respectively. The lines on the pole figures in the second column show the direction of fast-
510 shear wave polarization

References

Abers GA, van Keken PE, Kneller EA, et al (2006) The thermal structure of subduction zones constrained by seismic imaging: Implications for slab dehydration and wedge flow. Earth Planet Sci Lett 241:387–397. doi: 10.1016/j.epsl.2005.11.055

Babuška V, Fiala J, Kumazawa M, et al (1978) Elastic properties of garnet solid-solution series. Phys Earth Planet Inter 16:157–176. doi: 10.1016/0031-9201(78)90086-9

Boffa Ballaran T, Carpenter MA, Domeneghetti MC, Tazzoli V (1998) Structural mechanisms of solid solution and cation ordering in augite-jadeite pyroxenes: I. A macroscopic perspective.

Am Mineral 83:419–433.

Bascou J, Barruol G, Vauchez A, et al (2001) EBSD-measured lattice-preferred orientations and seismic properties of eclogites. Tectonophysics 342:61–80. doi: 10.1016/S0040-1951(01)00156-1

Bascou J, Tommasi A, Mainprice D (2002) Plastic deformation and development of clinopyroxene lattice preferred orientations in eclogites. J Struct Geol 24:1357–1368. doi: 10.1016/S0191-8141(01)00137-7

Bellaiche L, Vanderbilt D (2000) Virtual crystal approximation revisited: Application to dielectric and piezoelectric properties of perovskites. Phys Rev B 61:7877–7882. doi: 10.1103/PhysRevB.61.7877

Brenker FE, Prior DJ, Müller WF (2002) Cation ordering in omphacite and effect on deformation mechanism and lattice preferred orientation (LPO). J Struct Geol 24:1991–2005. doi: 10.1016/S0191-8141(02)00010-X

Browaeys JT, Chevrot S (2004) Decomposition of the elastic tensor and geophysical applications. Geophys J Int 159:667–678. doi: 10.1111/j.1365-246X.2004.02415.x

Burton BP, Davidson PM (1988) Short-range order and frustration in omphacite: Comparison of three CVM approximations. Phys Chem Miner 15:570–578. doi: 10.1007/BF00311028

Carpenter MA (1978) Kinetic control of ordering and exsolution in omphacite. Contrib Mineral Petrol 67:17–24. doi: 10.1007/BF00371629

Carpenter MA (1980) Mechanisms of exsolution in sodic pyroxenes. Contrib Mineral Petrol 71:289–300. doi: 10.1007/BF00371671

Collins MD, Brown JM (1998) Elasticity of an upper mantle clinopyroxene. Phys Chem Miner 26:7–13. doi: 10.1007/s002690050156

Cynn H, Anderson OL, Nicol M (1993) Effects of cation disordering in a natural MgAl2O4 spinel observed by rectangular parallelepiped ultrasonic resonance and Raman measurements. Pure Appl Geophys 141:415–444. doi: 10.1007/BF00998338

D'Arco P, Mustapha S, Ferrabone M, et al (2013) Symmetry and random sampling of symmetry independent configurations for the simulation of disordered solids. J Phys Condens Matter 25:355401. doi: 10.1088/0953-8984/25/35/355401

Dick BG, Overhauser AW (1958) Theory of the Dielectric Constants of Alkali Halide Crystals. Phys Rev 112:90–103. doi: 10.1103/PhysRev.112.90

Erba A, Mahmoud A, Orlando R, Dovesi R (2014) Elastic properties of six silicate garnet end members from accurate ab initio simulations. Phys Chem Miner 41:151–160. doi: 10.1007/s00269-013-0630-4

Faulkner J, Stocks G (1980) Calculating properties with the coherent-potential approximation. Phys

Rev B 21:3222–3244. doi: 10.1103/PhysRevB.21.3222

Gale JD (1997) GULP: A computer program for the symmetry-adapted simulation of solids. J Chem Soc Faraday Trans 93:629–637. doi: 10.1039/A606455H

Gale JD, Rohl AL (2003) The General Utility Lattice Program (GULP). Mol Simul 29:291–341. doi: 10.1080/0892702031000104887

Giannozzi P, Baroni S, Bonini N, et al (2009) QUANTUM ESPRESSO: a modular and open-source software project for quantum simulations of materials. J Phys Condens Matter 21:395502. doi: 10.1088/0953-8984/21/39/395502

Hazen RM, Yang H (1999) Effects of cation substitution and order-disorder on P-V-T equations of state of cubic spinels. Am Mineral 84:1956–1960.

Herzberg C (1995) Phase equilibria of common rocks in the crust and mantle. In: Ahrens TJ (ed) AGU Ref. Shelf. American Geophysical Union, Washington, D. C., pp 166–177

Hill R (1952) The Elastic Behaviour of a Crystalline Aggregate. Proc Phys Soc Sect A 65:349. doi: 10.1088/0370-1298/65/5/307

Hohenberg P, Kohn W (1964) Inhomogeneous Electron Gas. Phys Rev 136:B864–B871. doi: 10.1103/PhysRev.136.B864

Irifune T, Ringwood AE (1987) Phase transformations in a harzburgite composition to 26 GPa: implications for dynamical behaviour of the subducting slab. Earth Planet Sci Lett 86:365–376. doi: 10.1016/0012-821X(87)90233-0

Irifune T, Ringwood AE (1993) Phase transformations in subducted oceanic crust and buoyancy relationships at depths of 600–800 km in the mantle. Earth Planet Sci Lett 117:101–110. doi: 10.1016/0012-821X(93)90120-X

Irifune T, Sekine T, Ringwood AE, Hibberson WO (1986) The eclogite-garnetite transformation at high pressure and some geophysical implications. Earth Planet Sci Lett 77:245–256. doi: 10.1016/0012-821X(86)90165-2

Isaak DG, Ohno I, Lee PC (2006) The elastic constants of monoclinic single-crystal chrome-diopside to 1,300 K. Phys Chem Miner 32:691–699. doi: 10.1007/s00269-005-0047-9

Kandelin J, Weidner DJ (1988) The single-crystal elastic properties of jadeite. Phys Earth Planet Inter 50:251–260. doi: 10.1016/0031-9201(88)90106-9

Karki BB, Wentzcovitch RM, Gironcoli S de, Baroni S (1999) First-Principles Determination of Elastic Anisotropy and Wave Velocities of MgO at Lower Mantle Conditions. Science 286:1705–1707. doi: 10.1126/science.286.5445.1705

Kohn W, Sham LJ (1965) Self-Consistent Equations Including Exchange and Correlation Effects. Phys Rev 140:A1133–A1138. doi: 10.1103/PhysRev.140.A1133

Lacivita V, Erba A, Dovesi R, D'Arco P (2014) Elasticity of grossular–andradite solid solution: an ab initio investigation. Phys Chem Chem Phys 16:15331–15338. doi: 10.1039/C4CP01597E

Laks D, Ferreira L, Froyen S, Zunger A (1992) Efficient cluster expansion for substitutional systems. Phys Rev B 46:12587–12605. doi: 10.1103/PhysRevB.46.12587

Levien L, Prewitt CT (1981) High-pressure structural study of diopside. Am Mineral 66:315–323.

Levien L, Weidner DJ, Prewitt CT (1979) Elasticity of diopside. Phys Chem Miner 4:105–113. doi: 10.1007/BF00307555

Li B, Kung J, Liu W, Liebermann RC (2014) Phase transition and elasticity of enstatite under pressure from experiments and first-principles studies. Phys Earth Planet Inter 228:63–74. doi: 10.1016/j.pepi.2013.11.009

Li B, Neuville DR (2010) Elasticity of diopside to 8 GPa and 1073 K and implications for the upper mantle. Phys Earth Planet Inter 183:398–403. doi: 10.1016/j.pepi.2010.08.009

Li L, Carrez P, Weidner D (2007a) Effect of cation ordering and pressure on spinel elasticity by ab initio simulation. Am Mineral 92:174–178. doi: 10.2138/am.2007.2210

Li L, Weidner DJ, Brodholt J, Price GD (2007b) The effect of cation-ordering on the elastic properties of majorite: An ab initio study. Earth Planet Sci Lett 256:28–35. doi: 10.1016/j.epsl.2007.01.008

Luo F, Cheng Y, Cai L-C, Chen X-R (2013) Structure and thermodynamic properties of BeO: Empirical corrections in the quasiharmonic approximation. J Appl Phys 113:033517. doi: 10.1063/1.4776679

Mainprice D (2007) Seismic Anisotropy of the Deep Earth from a Mineral and Rock Physics Perspective. In: Price GD (eds) Treatise on Geophysics, Volume 2: Mineral Physics. Elsevier, Amsterdam, pp 437–491

Mainprice D, Bascou J, Cordier P, Tommasi A (2004) Crystal preferred orientations of garnet: comparison between numerical simulations and electron back-scattered diffraction (EBSD) measurements in naturally deformed eclogites. J Struct Geol 26:2089–2102. doi: 10.1016/j.jsg.2004.04.008

Matsui M, Busing WR (1984) Calculation of the elastic constants and high-pressure properties of diopside, CaMgSi 2 O 6. Am Mineral 69:1090–1095.

Mauler A, Burlini L, Kunze K, et al (2000) P-wave anisotropy in eclogites and relationship to the omphacite crystallographic fabric. Phys Chem Earth Part Solid Earth Geod 25:119–126. doi: 10.1016/S1464-1895(00)00020-X

Mauler A, Godard G, Kunze K (2001) Crystallographic fabrics of omphacite, rutile and quartz in Vendée eclogites (Armorican Massif, France). Consequences for deformation mechanisms and regimes. Tectonophysics 342:81–112. doi: 10.1016/S0040-1951(01)00157-3

Moakher M, Norris AN (2006) The Closest Elastic Tensor of Arbitrary Symmetry to an Elasticity Tensor of Lower Symmetry. J Elast 85:215–263. doi: 10.1007/s10659-006-9082-0

Momma K, Izumi F (2011) *VESTA 3* for three-dimensional visualization of crystal, volumetric and morphology data. J Appl Crystallogr 44:1272–1276. doi: 10.1107/S0021889811038970

Monkhorst HJ, Pack JD (1976) Special points for Brillouin-zone integrations. Phys Rev B 13:5188–5192. doi: 10.1103/PhysRevB.13.5188

Mustapha S, D'Arco P, Pierre MDL, et al (2013) On the use of symmetry in configurational analysis for the simulation of disordered solids. J Phys Condens Matter 25:105401. doi: 10.1088/0953-8984/25/10/105401

Oganov AR, Brodholt JP, Price GD (2001) Ab initio elasticity and thermal equation of state of MgSiO3 perovskite. Earth Planet Sci Lett 184:555–560. doi: 10.1016/S0012-821X(00)00363-0

O'Neill B, Bass JD, Smyth JR, Vaughan MT (1989) Elasticity of a grossular-pyrope-almandine garnet. J Geophys Res Solid Earth 94:17819–17824. doi: 10.1029/JB094iB12p17819

Otero-de-la-Roza A, Abbasi-Pérez D, Luaña V (2011) Gibbs2: A new version of the quasiharmonic model code. II. Models for solid-state thermodynamics, features and implementation. Comput Phys Commun 182:2232–2248. doi: 10.1016/j.cpc.2011.05.009

Otero-de-la-Roza A, Luaña V (2011a) Treatment of first-principles data for predictive quasiharmonic thermodynamics of solids: The case of MgO. Phys Rev B 84:024109. doi: 10.1103/PhysRevB.84.024109

Otero-de-la-Roza A, Luaña V (2011b) Equations of state and thermodynamics of solids using empirical corrections in the quasiharmonic approximation. Phys Rev B 84:184103. doi: 10.1103/PhysRevB.84.184103

Pandolfo F, Cámara F, Domeneghetti MC, et al (2014) Volume thermal expansion along the jadeite–diopside join. Phys Chem Miner doi: 10.1007/s00269-014-0694-9

Panero WR (2008) Cation disorder in ringwoodite and its effects on wave speeds in the Earth's transition zone. J Geophys Res Solid Earth 113:B10204. doi: 10.1029/2008JB005676

Pavese A, Bocchio R, Ivaldi G (2000) In situ high temperature single crystal X-ray diffraction study of a natural omphacite. Mineral Mag 64:983–993.

Pavese A, Diella V, Levy D, Hanfland M (2001) Synchrotron X-ray powder diffraction study of natural P2 /n-omphacites at high-pressure conditions. Phys Chem Miner 28:9–16. doi: 10.1007/s002690000128

Peacock SM, Keken PE van, Holloway SD, et al (2005) Thermal structure of the Costa Rica – Nicaragua subduction zone. Phys Earth Planet Inter 149:187–200. doi: 10.1016/j.pepi.2004.08.030

Peacock SM, Wang K (1999) Seismic Consequences of Warm Versus Cool Subduction Metamorphism: Examples from Southwest and Northeast Japan. Science 286:937–939. doi: 10.1126/science.286.5441.937

Perdew JP (1991) Unified Theory of Exchange and Correlation Beyond the Local Density Approximation. In: Ziesche P, Eschrig H (eds)Akademie Verlag, Berlin, pp 11–20

Perdew JP, Burke K, Ernzerhof M (1996) Generalized Gradient Approximation Made Simple. Phys Rev Lett 77:3865–3868. doi: 10.1103/PhysRevLett.77.3865

Perdew JP, Chevary JA, Vosko SH, et al (1992) Atoms, molecules, solids, and surfaces: Applications of the generalized gradient approximation for exchange and correlation. Phys Rev B 46:6671–6687. doi: 10.1103/PhysRevB.46.6671

Perger WF, Criswell J, Civalleri B, Dovesi R (2009) Ab-initio calculation of elastic constants of crystalline systems with the CRYSTAL code. Comput Phys Commun 180:1753–1759. doi: 10.1016/j.cpc.2009.04.022

Ranganathan SI, Ostoja-Starzewski M (2008) Universal Elastic Anisotropy Index. Phys Rev Lett 101:055504. doi: 10.1103/PhysRevLett.101.055504

Rossi G, Smith DC, Ungaretti L, Domeneghetti MC (1983) Crystal-chemistry and cation ordering in the system diopside-jadeite: A detailed study by crystal structure refinement. Contrib Mineral Petrol 83:247–258. doi: 10.1007/BF00371193

Saha S, Zwanziger JW (2014) Elastic properties of ternary (Alx,Mg1−x)Sc random alloys from first principles methods. J Alloys Compd 610:138–142. doi: 10.1016/j.jallcom.2014.04.102

Sang L, Bass JD (2014) Single-crystal elasticity of diopside to 14 GPa by Brillouin scattering. Phys Earth Planet Inter 228:75–79. doi: 10.1016/j.pepi.2013.12.011

Sondergeld P, Li B, Schreuer J, Carpenter MA (2006) Discontinuous evolution of single-crystal elastic constants as a function of pressure through the C2/c ↔ P21/c phase transition in spodumene (LiAlSi2O6). J Geophys Res Solid Earth 111:B07202. doi: 10.1029/2005JB004098

Stackhouse S, Brodholt JP, Wookey J, et al (2005) The effect of temperature on the seismic anisotropy of the perovskite and post-perovskite polymorphs of MgSiO3. Earth Planet Sci Lett 230:1–10. doi: 10.1016/j.epsl.2004.11.021

Syracuse EM, van Keken PE, Abers GA (2010) The global range of subduction zone thermal models. Phys Earth Planet Inter 183:73–90. doi: 10.1016/j.pepi.2010.02.004

Tasnádi F, Odén M, Abrikosov IA (2012) Ab initio elastic tensor of cubic Ti0.5Al0.5N alloys: Dependence of elastic constants on size and shape of the supercell model and their convergence. Phys Rev B 85:144112. doi: 10.1103/PhysRevB.85.144112

Ulrich S, Mainprice D (2005) Does cation ordering in omphacite influence development of lattice-preferred orientation? J Struct Geol 27:419–431. doi: 10.1016/j.jsg.2004.11.003

Vanderbilt D (1998) First-principles theory of structural phase transitions in cubic perovskites. J Korean Phys Soc 32:S103–S106.

Vanderbilt D (1990) Soft self-consistent pseudopotentials in a generalized eigenvalue formalism. Phys Rev B 41:7892–7895. doi: 10.1103/PhysRevB.41.7892

Van de Walle A (2008) A complete representation of structure–property relationships in crystals. Nat Mater 7:455–458. doi: 10.1038/nmat2200

Van de Walle A (2009) Multicomponent multisublattice alloys, nonconfigurational entropy and other additions to the Alloy Theoretic Automated Toolkit. Calphad 33:266–278. doi: 10.1016/j.calphad.2008.12.005

Van de Walle A, Asta M, Ceder G (2002) The alloy theoretic automated toolkit: A user guide. Calphad 26:539–553. doi: 10.1016/S0364-5916(02)80006-2

Van de Walle A, Ceder G (1999) Correcting overbinding in local-density-approximation calculations. Phys Rev B 59:14992–15001. doi: 10.1103/PhysRevB.59.14992

Van de Walle A, Tiwary P, de Jong M, et al (2013) Efficient stochastic generation of special quasirandom structures. Calphad 42:13–18. doi: 10.1016/j.calphad.2013.06.006

Vinograd VL (2002a) Thermodynamics of mixing and ordering in the diopside–jadeite system: I. A CVM model. Mineral Mag 66:513–536. doi: 10.1180/0026461026640046

Vinograd VL (2002b) Thermodynamics of mixing and ordering in the diopside –jadeite system: II. A polynomial fit to the CVM results. Mineral Mag 66:537–545. doi: 10.1180/0026461026640047

Vinograd VL, Gale JD, Winkler B (2007) Thermodynamics of mixing in diopside–jadeite, CaMgSi2O6–NaAlSi2O6, solid solution from static lattice energy calculations. Phys Chem Miner 34:713–725. doi: 10.1007/s00269-007-0189-z

Vinograd VL, Sluiter MHF, Winkler B, Putnis A, Gale JD (2004) Thermodynamics of mixing and ordering in silicates and oxides from static lattice energy and ab initio calculations. In: Warren M, Oganov A, Winkler B (eds) First-principles simulations: perspectives and challenges in mineral sciences (Deutsche Gesellschaft fur Kristallographie. Berichte aus Arbeitskreisen der DFK) 14, pp 143–151

Vinograd VL, Winkler B, Putnis A, et al (2006) Thermodynamics of pyrope–majorite, Mg3Al2Si3O12–Mg4Si4O12, solid solution from atomistic model calculations. Mol Simul 32:85–99. doi: 10.1080/08927020500501599

Walker AM (2012) The effect of pressure on the elastic properties and seismic anisotropy of diopside and jadeite from atomic scale simulation. Phys Earth Planet Inter 192–193:81–89. doi: 10.1016/j.pepi.2011.10.002

Walker AM, Tyer RP, Bruin RP, Dove MT (2008) The compressibility and high pressure structure of diopside from first principles simulation. Phys Chem Miner 35:359–366. doi:

10.1007/s00269-008-0229-3

Walker AM, Wookey J (2012) MSAT—A new toolkit for the analysis of elastic and seismic anisotropy. Comput Geosci 49:81–90. doi: 10.1016/j.cageo.2012.05.031

Wentzcovitch RM, Martins JL, Price GD (1993) Ab initio molecular dynamics with variable cell shape: Application to MgSiO3. Phys Rev Lett 70:3947–3950. doi: 10.1103/PhysRevLett.70.3947

Wentzcovitch RM, Ross NL, Price GD (1995) Ab initio study of MgSiO3 and CaSiO3 perovskites at lower-mantle pressures. Phys Earth Planet Inter 90:101–112. doi: 10.1016/0031-9201(94)03001-Y

Xie M-Y, Tasnádi F, Abrikosov IA, et al (2012) Elastic constants, composition, and piezolectric polarization in InxAl1−xN: From ab initio calculations to experimental implications for the applicability of Vegard's rule. Phys Rev B 86:155310. doi: 10.1103/PhysRevB.86.155310

Zhang J, Green HW (2007) Experimental Investigation of Eclogite Rheology and Its Fabrics at High Temperature and Pressure. J Metamorph Geol 25:97–115. doi: 10.1111/j.1525-1314.2006.00684.x

Zhou L, Holec D, Mayrhofer PH (2013) First-principles study of elastic properties of cubic Cr1−xAlxN alloys. J Appl Phys 113:043511. doi: 10.1063/1.4789378

Zunger A, Wei S-H, Ferreira LG, Bernard JE (1990) Special quasirandom structures. Phys Rev Lett 65:353–356. doi: 10.1103/PhysRevLett.65.353

511 **Table 1** Elastic constants (in GPa) of P2/n omphacite at 0 GPa applied pressure calculated using
512 plane-wave DFT, compared with values for jadeite and diopside taken from Walker (2012). Bulk
513 and shear moduli are the Voigt-Reuss-Hill averages (Hill 1952)

	Diopside[a]	Jadeite[a]	Linear-Mixing[b]	P2/n omphacite	Difference[c]
C_{11}	212.3(11)	243.6(25)	228.0(14)	235.6(11)	-7.6(18)
C_{22}	158.0(11)	228.1(17)	193.1(10)	193.4(24)	-0.3(26)
C_{33}	226.3(15)	266.2(24)	246.3(14)	245.4(13)	0.9(20)
C_{44}	65.3(6)	79.5(4)	72.4(4)	71.4(3)	1.0(5)
C_{55}	61.9(1)	64.6(4)	63.3(2)	67.1(9)	-3.8(9)
C_{66}	69.3(5)	85.7(12)	77.5(7)	79.4(4)	-1.9(8)
C_{12}	69.8(7)	77.4(9)	73.6(6)	81.3(5)	-7.7(8)
C_{13}	60.6(9)	56.1(10)	58.4(7)	69.0(8)	-10.6(11)
C_{23}	50.7(4)	73.5(3)	62.1(3)	57.1(6)	5.0(7)
C_{15}	15.4(3)	11.7(9)	13.6(5)	14.0(4)	-0.4(6)
C_{25}	10.0(1)	14.0(2)	12.0(1)	14.9(6)	-2.9(6)
C_{35}	54.9(3)	37.8(6)	46.4(3)	50.1(6)	-3.7(7)

C_{46}	10.8(4)	14.5(3)	12.5(3)	11.4(2)	1.1(4)
K^h	99.8(4)	124.5(6)	112.5(4)	115.1(5)	-2.6(6)
G^h	63.5(2)	78.9(3)	71.5(2)	72.0(3)	-0.5(4)

[a] Elastic constants at 0 GPa applied pressure calculated using DFT, from Walker (2012)

[b] Compositionally weighted linear mixing of elastic constants of diopside and jadeite

[c] Difference between the elastic constants of omphacite predicted from linear mixing and those calculated using DFT

Table 2 Elastic constants (in GPa) of P2/n omphacite, diopside, and jadeite calculated in GULP using the interatomic potential from Vinograd et al. (2007), as well as for the 4x4x4 SQS supercells of omphacite for the two cation disorder cases considered: mixing over M2 only, and mixing over both cation sites. The elastic constants calculated using the mean field method (Gale and Rohl 2003) have also been included, and the often substantial difference between these and the elastic constants calculated for the SQS supercells illustrate the importance of local structural relaxation in solid solutions

	Diopside	Jadeite	Linear-mixing	P2/n omphacite	Difference	Mixing on M2 only		Mixing on M1 and M2	
						Mean field	SQS	Mean field	SQS
C_{11}	222.6	245.7	234.1	234.0	0.1	235.1	233.1	237.3	228.7
C_{22}	166.5	226.8	196.7	198.3	-1.6	193.1	189.5	200.6	188.2
C_{33}	236.3	287.6	262.0	261.9	0.1	263.4	258.9	263.4	257.0
C_{44}	63.3	67.4	65.4	64.5	0.9	64.3	60.6	65.0	61.8
C_{55}	62.3	53.0	57.7	64.5	-6.8	62.8	62.8	63.2	59.2
C_{66}	65.2	75.5	70.4	72.0	-1.6	72.9	70.0	74.6	66.9
C_{12}	76.5	85.1	80.8	85.4	-4.6	83.1	84.8	86.1	81.6
C_{13}	73.9	78.7	76.3	83.0	-6.7	80.3	80.0	80.8	78.8
C_{23}	62.1	92.9	77.5	71.8	5.7	76.2	72.3	75.5	74.5
C_{15}	19.2	16.0	17.6	21.7	-4.1	19.8	15.9	18.7	17.3

C_{25}	8.7	24.4	16.5	17.3	-0.8	15.6	14.0	14.5	15.0
C_{35}	51.9	35.0	43.5	48.1	-4.6	44.0	42.3	44.7	39.7
C_{46}	10.6	19.9	15.3	14.4	0.9	12.4	12.3	13.4	13.0
K^h	110.3	135.2	122.8	123.6	-0.8	124.1	123.3	126.2	121.8
G^h	62.8	69.3	66.1	68.0	-1.9	67.9	66.1	68.8	64.7

514

Figure

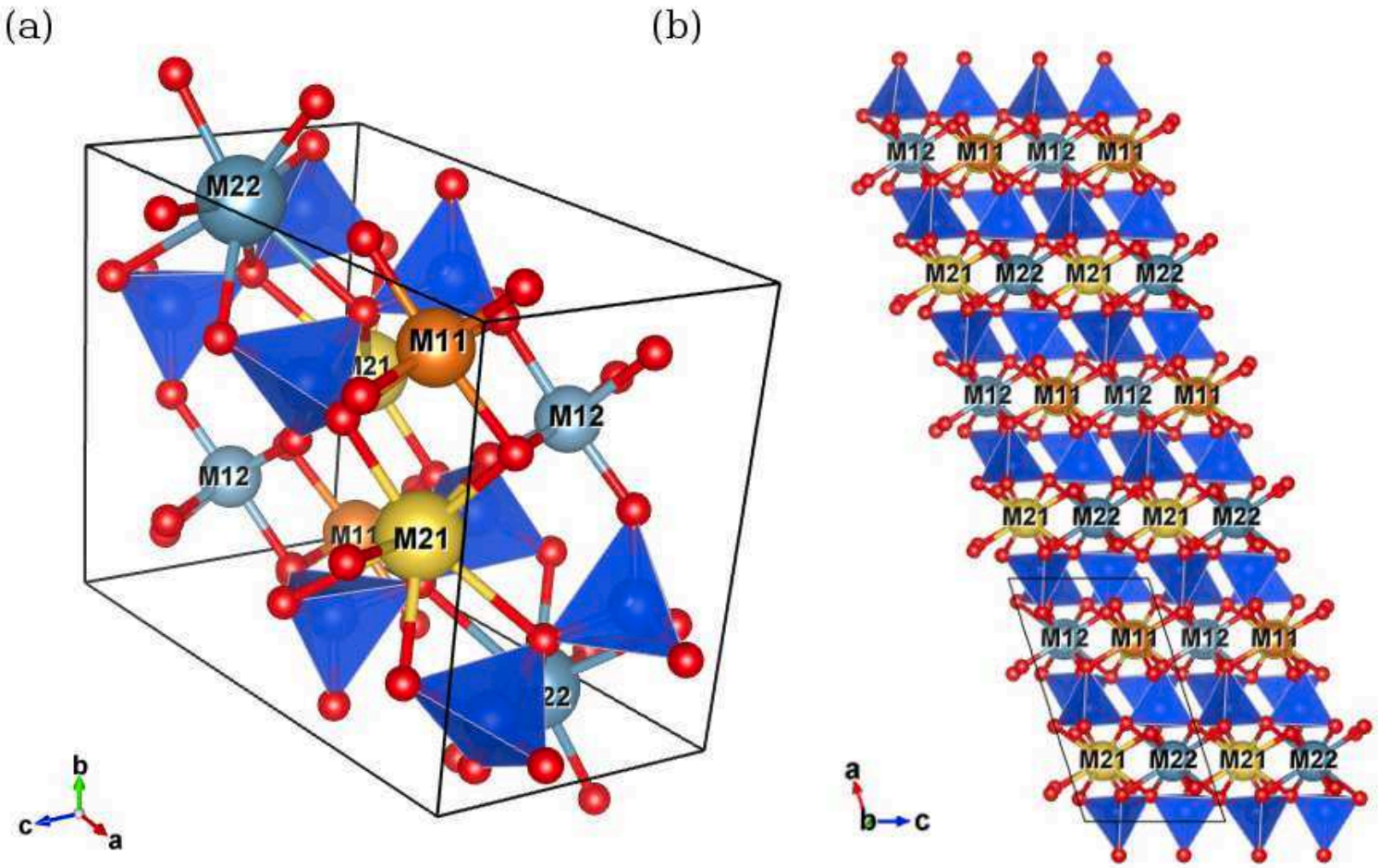
(a)
(b)
M22
M11
M12
M12
M11
M21
M12
M11
M12
M11
M21
M22
M21
M22
M12
M11
M12
M11
M21
M22
M21
M22
M12
M11
M12
M11
M21
M22
M21
M22
b
c
a
a
b
c

Figure

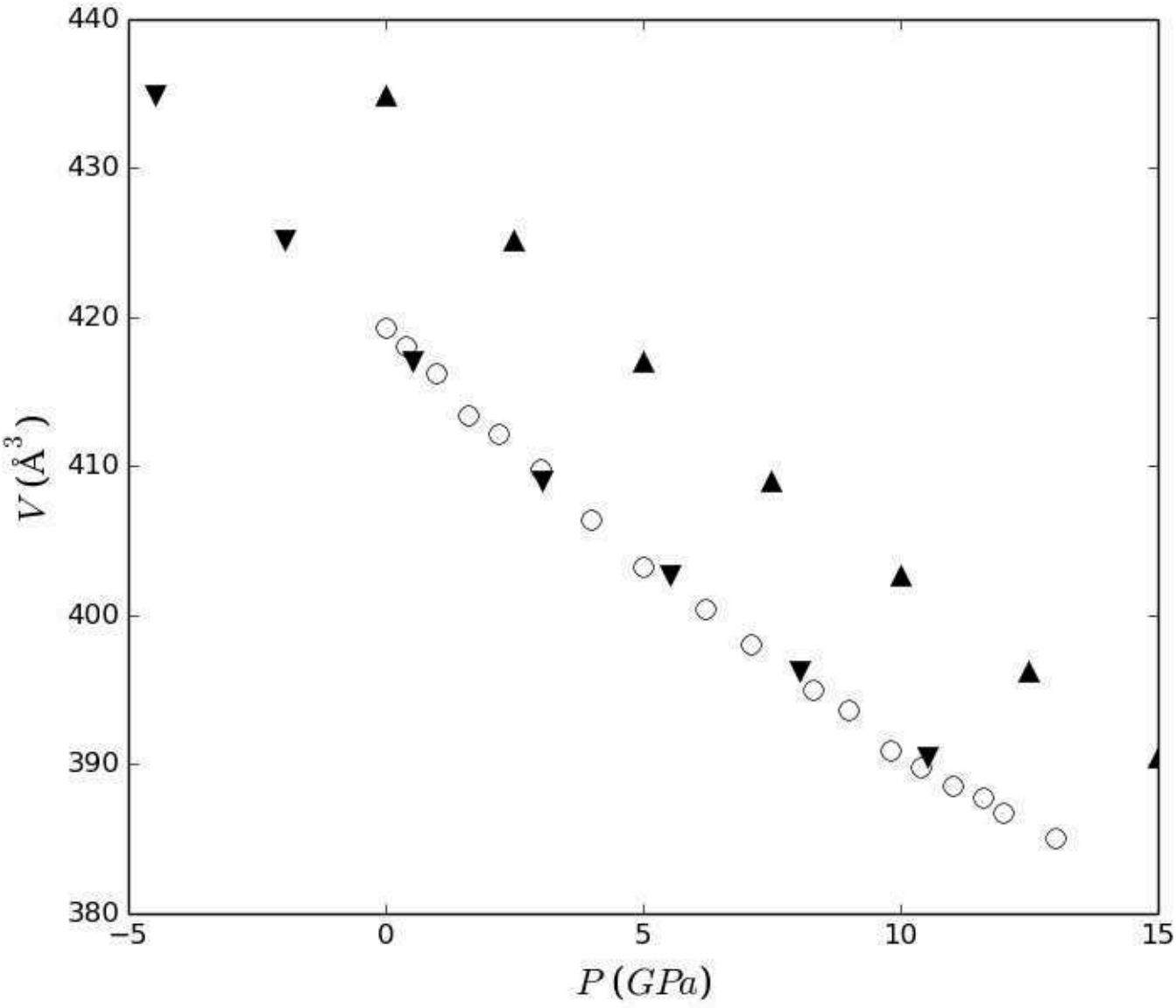

Figure

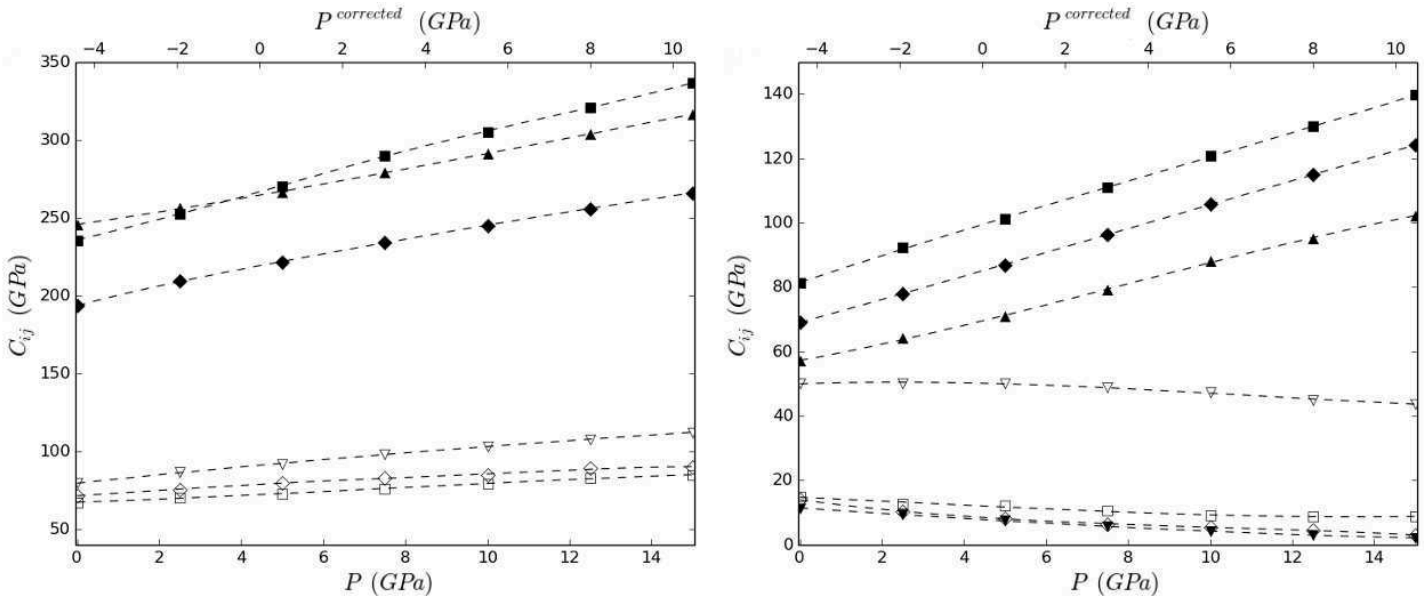

Figure

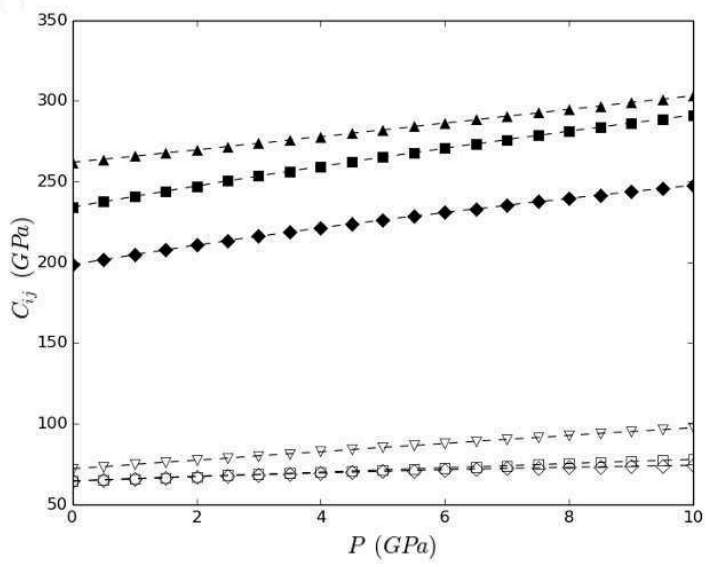
350
300
250
200
150
100
50
0
2
4
6
8
10
C_{ij} (GPa)
P (GPa)

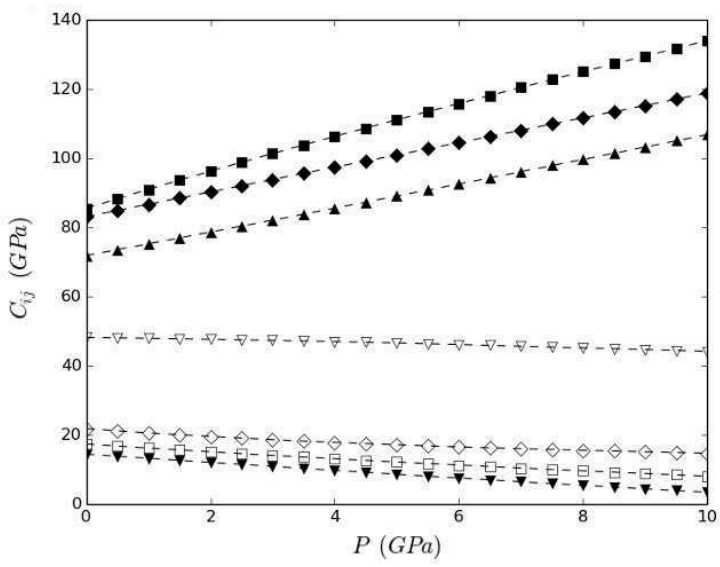
140
120
100
80
60
40
20
0
2
4
6
8
10
C_{ij} (GPa)
P (GPa)

Figure

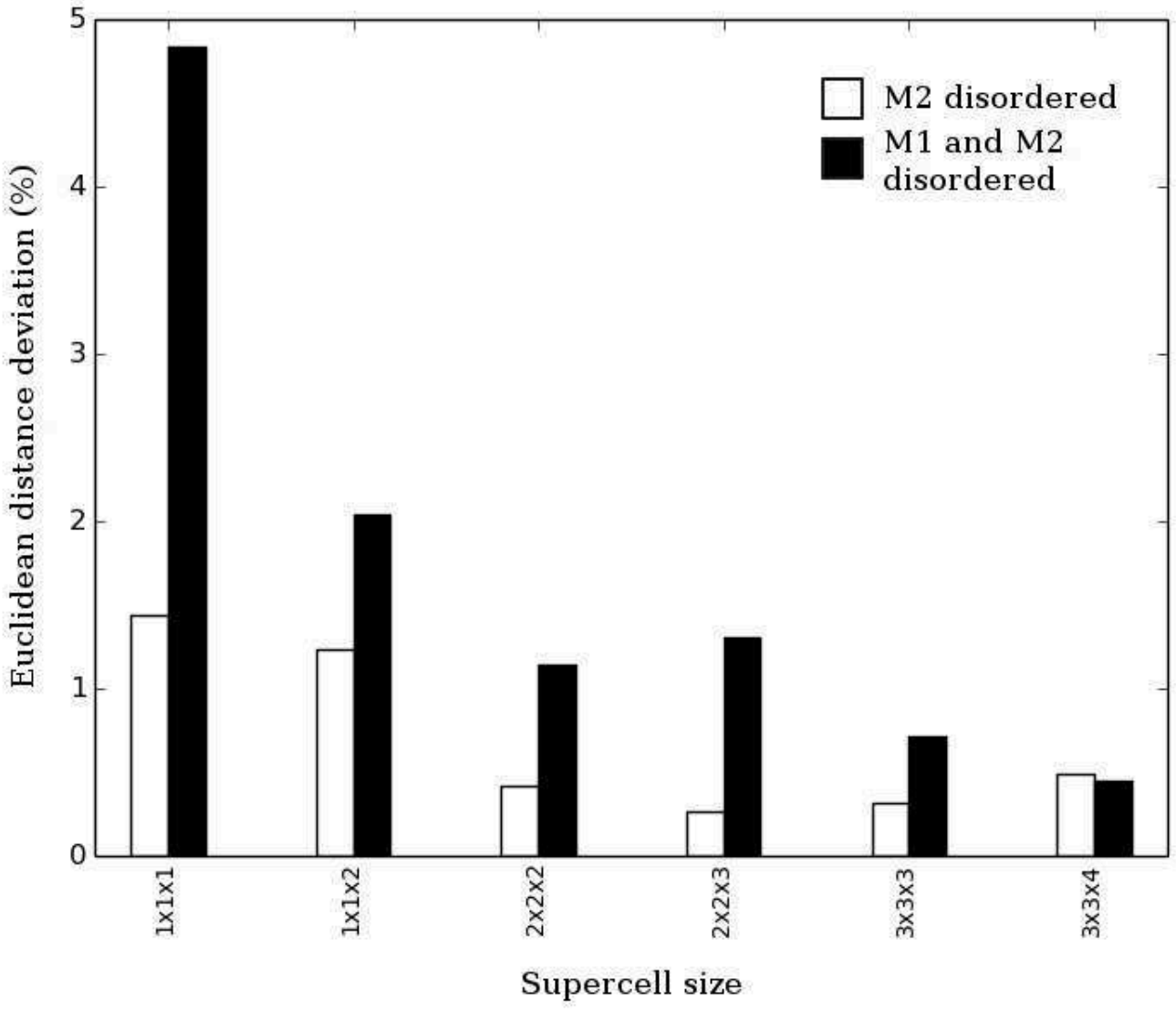
M2 disordered
M1 and M2 disordered
Euclidean distance deviation (%)
0
1
2
3
4
5
1x1x1
1x1x2
2x2x2
2x2x3
3x3x3
3x3x4
Supercell size

Figure

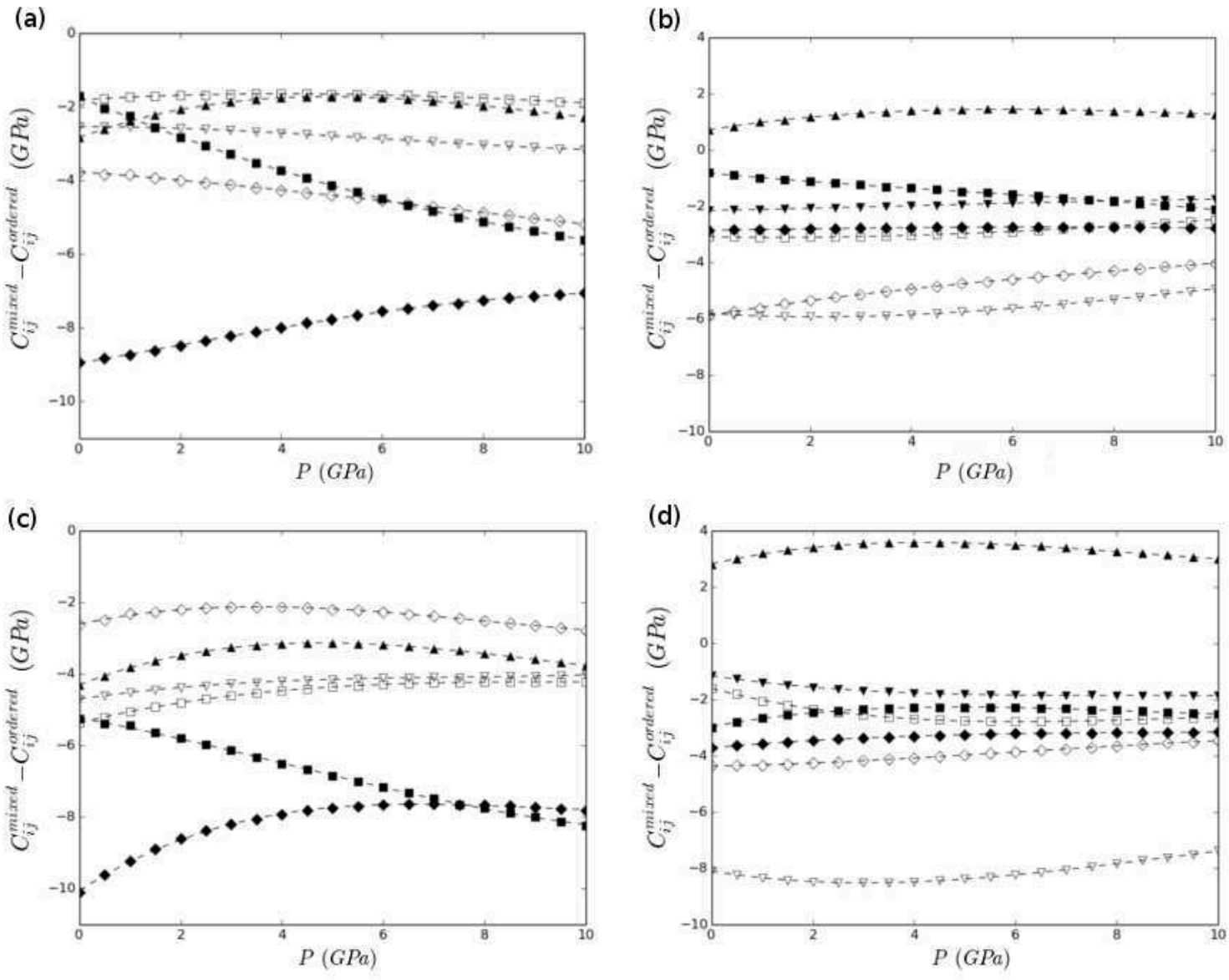

Figure

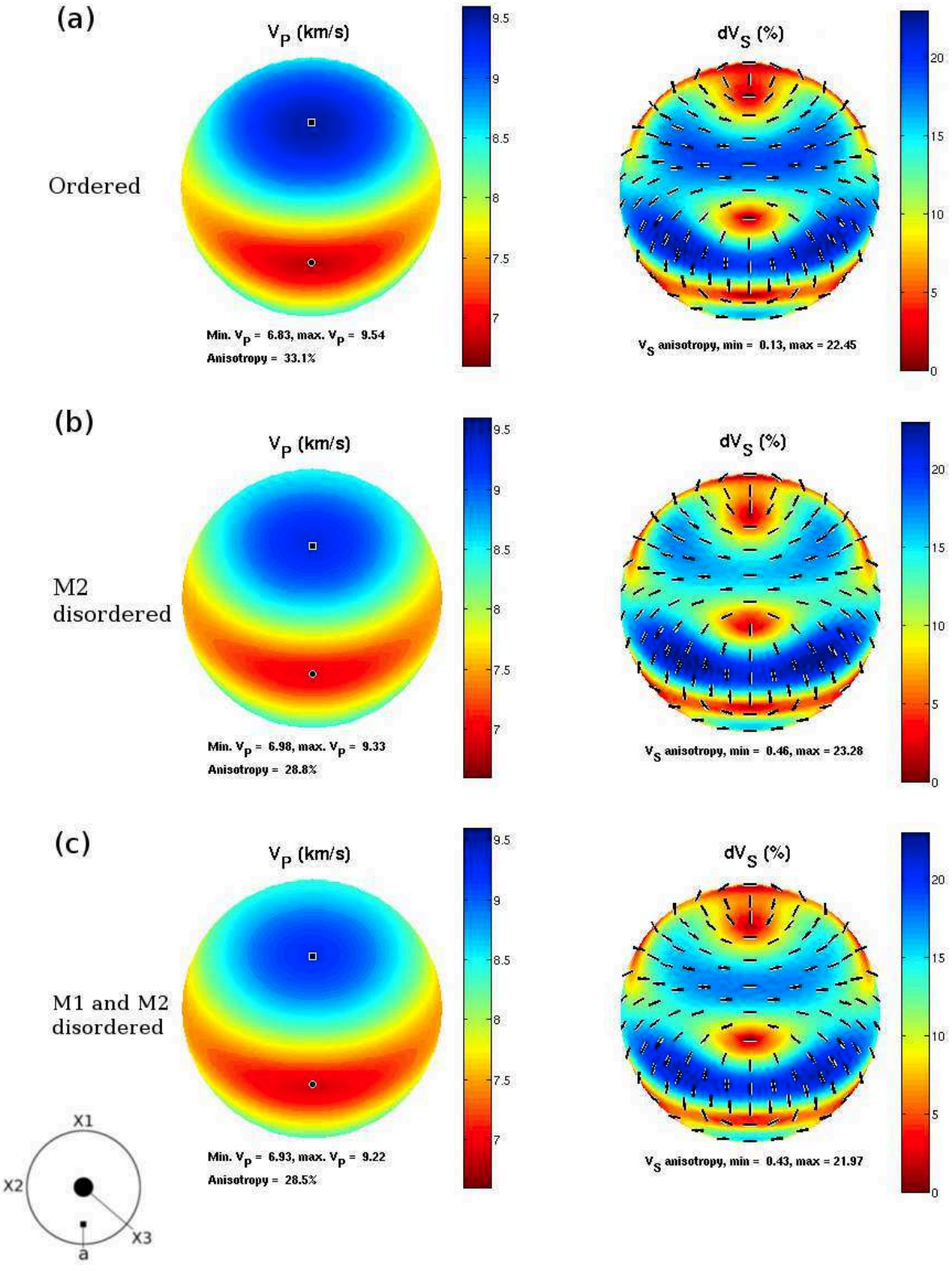
(a)
Ordered
V_P (km/s)
9.5
9
8.5
8
7.5
7
Min. V_P = 6.83, max. V_P = 9.54
Anisotropy = 33.1%
dV_S (%)
20
15
10
5
0
V_S anisotropy, min = 0.13, max = 22.45
(b)
M2
disordered
V_P (km/s)
9.5
9
8.5
8
7.5
7
Min. V_P = 6.98, max. V_P = 9.33
Anisotropy = 28.8%
dV_S (%)
20
15
10
5
0
V_S anisotropy, min = 0.46, max = 23.28
(c)
M1 and M2
disordered
V_P (km/s)
9.5
9
8.5
8
7.5
7
Min. V_P = 6.93, max. V_P = 9.22
Anisotropy = 28.5%
dV_S (%)
20
15
10
5
0
V_S anisotropy, min = 0.43, max = 21.97
X1
X2
X3
a